ARCHIVIO ISTITUZIONALE
DELLA RICERCA

Alma Mater Studiorum Università di Bologna
Archivio istituzionale della ricerca

Thermodynamically versus Kinetically Controlled Self-Assembly of a Naphthalenediimide-Thiophene Derivative: From Crystalline, Fluorescent, n-Type Semiconducting 1D Needles to Nanofibers

This is the final peer-reviewed author's accepted manuscript (postprint) of the following publication:

Published Version:
Zangoli, M., Gazzano, M., Monti, F., Maini, L., Gentili, D., Liscio, A., et al. (2019). Thermodynamically versus Kinetically Controlled Self-Assembly of a Naphthalenediimide-Thiophene Derivative: From Crystalline, Fluorescent, n-Type Semiconducting 1D Needles to Nanofibers. ACS APPLIED MATERIALS & INTERFACES, 11(18), 16864-16871 [10.1021/acsami.9b02404].

Availability:
This version is available at: https://hdl.handle.net/11585/686992 since: 2020-02-27

Published:

DOI: http://doi.org/10.1021/acsami.9b02404

Terms of use:

Some rights reserved. The terms and conditions for the reuse of this version of the manuscript are specified in the publishing policy. For all terms of use and more information see the publisher's website.

This item was downloaded from IRIS Università di Bologna (https://cris.unibo.it/).
When citing, please refer to the published version.

(Article begins on next page)

06 October 2026

Thermodynamically vs Kinetically Controlled Self-assembly of a Naphthalenediimide-thiophene Derivative: from Crystalline, Fluorescent, n-type Semiconducting 1D Needles to Nanofibers

Mattia Zangoli[§ζǁ], Massimo Gazzano[§ǁ], Filippo Monti[§ǁ], Lucia Maini[†], Denis Gentili[#], Andrea Liscio[Δ], Alberto Zanelli[§], Elisabetta Salatelli[±], Giuseppe Gigli[&], Massimo Baroncini[¥§], Francesca Di Maria[&§]**

[&] CNR-NANOTEC, c/o Campus Ecotekne – University of Salento, via Monteroni, I-73100 Lecce, Italy
[§] CNR-ISOF, Via P. Gobetti 101, I-40129 Bologna, Italy
[ζ] Mediteknology srl, Via P. Gobetti 101, I-40129, Bologna, Italy
[¥] Dpt. of Agricultural and Food Sciences - DISTAL, University of Bologna, Viale Fanin 44, I-40126 Bologna, Italy
[#] CNR-ISMN, Via P. Gobetti 101, I-40129 Bologna, Italy
[†] Dpt. of Chemistry Giacomo Ciamician, University of Bologna, Via Selmi 2, I-40126 Bologna, Italy
[Δ] CNR-IMM, Via del Fosso del Cavaliere 100, I-00133 Roma, Italy
[±] Dpt. of Industrial Chemistry Toso Montanari, University of Bologna, Viale del Risorgimento 4, I-40136 Bologna, Italy

KEYWORDS: supramolecular architectures, kinetic control, polymorphs, n-type organic semiconductors, solid-state luminescent enhancement.

ABSTRACT

The control over aggregation pathways is a key requirement for present and future technologies, as it can provide access to a variety of sophisticated structures with unique functional properties. In the present work we demonstrate an unprecedented control over the supramolecular self-assembly of a semiconductive material – based on a naphthalenediimide (NDI) core functionalized with phenyl-thiophene moieties at the imide termini (ThPh-NDI) – by trapping the molecules into different arrangements depending on the crystallization conditions. The control of the solvent evaporation rate enables to grow highly elaborate hierarchical self-assembled structures: either in an energy-minimum thermodynamic state when the solvent is slowly evaporated forming needles shaped crystals (polymorph α), or in a local energy-minimum state when the solvent is rapidly evaporated leading to the formation of nanofibers (polymorph β). The exceptional persistence of the kinetically trapped β form allowed the study and comparison of its characteristics with that of the stable α form, revealing the importance of molecular aggregation geometry on functional properties. Intriguingly, we found that compared to the thermodynamically stable α phase, characterized by a J-type aggregation, the β phase exhibits: i) an unusual strong blue shift of the emission from the charge transfer state responsible of the solid-state luminescent enhancement (SSE), ii) a higher work function with a "rigid shift" of the electronic levels, as shown by kelvin probe force microscopy and cyclic voltammetry measurements and iii) a superior FET mobility in agreement with a H-type aggregation as indicated by X-ray analysis and theoretical calculations.

INTRODUCTION

Supramolecular self-assembly of π-systems driven by non-covalent interactions has gained an increasing interest in interdisciplinary research areas, ranging from organic electronic to biology, as a *bottom up* approach to create novel nano- and microstructures with a programmed geometry and tailored physicochemical properties.[1-6] The possibility of integrating these self-organized supramolecular architectures directly into electronic devices is an even more important challenge for the development of modern nanotechnology.[7-10] For these reasons determining the factors that regulate/influence self-assembly has become increasingly important to direct the process itself.[11,12] Typically, the control over self-assembly relies on molecular engineering by the rational introduction of selected functionalities/building blocks, that drive and control molecular recognition through specific weak interactions leading to the formation of supramolecular assemblies under thermodynamic control.[13,14] However, the outcome of aggregation processes is also dependent on 'environmental factors', indeed it is well known that even a small variation in the experimental conditions may alter the subtle balance among the different attractive/repulsive forces inducing structural modifications in the final assemblies.[15-22] This allows to strategically expand the usefulness of the molecules by obtaining from a single species a wide range of materials with distinct molecular arrangements, namely polymorphs, thus achieving a dynamic tuning of their solid state properties.[23-25] In this context, kinetic factors must be considered to further expand and control the self-assembly process, hence shedding light on the interplay between thermodynamics and kinetics can provide novel routes towards tailoring molecular structure formation. In this work we demonstrate the importance of kinetic effects in modulating the self-assembly characteristics of a Naphthalene diimides derivative (NDI) – a member belonging to a broader class of compounds called rylenes known as promising candidates for

organic electronics applications[26-28] that enable a precise and reproducible control over material properties and functions. We found that depending on the temperature of the substrate employed during the deposition process, it is possible to selectively and reproducibly prepare two different polymorphic one-dimensional (1D) nanostructures: needle shaped crystals, the polymorph confined in the lowest energy thermodynamic equilibrium state (polymorph α), and nanofibers, the polymorph kinetically trapped in a local minimum of the energetic landscape (polymorph β). Owing to the capability of performing a suitable polymorph selection, the two nanostructures were analyzed in depth by different techniques: UV-vis and photoluminescence spectroscopy, Differential Scanning Calorimetry (DSC), Cyclic Voltammetry (CV) and Kelvin Probe Force Microscopy (KPFM). We demonstrate that the different optical, electronic and charge transport properties between the two polymorphs are determined by their different molecular packing at the molecular scale, either J- or H-type, as indicated by X-ray analysis and theoretical calculations. Moreover, we show that the kinetically trapped β phase can be successfully employed for fabricating air-stable OFET devices thanks to its persistence, i.e. it resides stably in its local energy minimum preventing phase transitions for a time-length exceeding the lifetime of the device itself, and its superior performances compared to the thermodynamic one.

RESULTS AND DISCUSSION

Polymorphic nanostructures formation. The NDI-thiophene derivative (**ThPh-NDI**) was synthesized according to scheme S1 (see SI). Compared to the procedures described in the literature for this family of compounds,[29-30] the implementation of microwave irradiation in the condensation step – between naphthalene-1,4,5,8-tetracarboxylic dianhydride and the amine derivative – ensured a drastic increase in the yield and a concomitant reduction in reaction time,

from hours to minutes. Polymorphic nanostructures are grown by dissolving **ThPh-NDI** in DMF (~ 10^{-6} M) at a temperature of about 40°C to favor its complete dissolution, given the tendency to self-aggregate despite the presence of solubilizing alkyl chains, and by drop casting the solution onto a substrate placed on a hot plate kept at a constant temperature (Fig. 1). Thermal analysis show that **ThPh-NDI**, in both polymorphic forms, is thermally stable and decomposes only at temperature higher than 300°C (Fig. S1). Depending on the temperature at which the substrate is held, the aggregation pathway changes and the two nanostructures can be reproducibly grown in different substrates with a high phase purity. As shown in Figure 1, setting the temperature of the substrate below 40°C leads to a slow evaporation of the DMF solution of **ThPh-NDI**, bringing about the formation of needle shaped crystals, namely polymorph α. Instead, a rapid evaporation of the DMF solution induced by maintaining the temperature of the substrate above 150°C, a temperature close to the solvent boiling point, bring about the formation of longer and thinner crystalline nanofibers, namely polymorph β. While slow evaporation conditions allow for a complete equilibration leading to the formation of the thermodynamic polymorph, i.e. the one residing in the energy minimum, fast evaporation allows to kinetically trap the system in a local energy minimum. i.e. forming a metastable polymorph. In the latter case, according to Ostwald's step rules, the high degree of supersaturation achieved reduces the possibility of converting the metastable form nucleating first into the more thermodynamically stable form through solution-mediated transformation.[31] In agreement, the two forms display different solubility at room temperature in DMF; indeed, while polymorph α is scarcely soluble remaining almost undissolved, polymorph β shows a marked solubility typical of metastable forms ($\Delta G_{\alpha \rightarrow \beta} > 0$) being completely dissolved. Optical photomicrographs well illustrate the different crystal morphology of the two forms: polymorph α shows a short prismatic crystalline habit, with

individual crystals less than 200 micrometers in length and comparable width and thickness (Fig. 1A-C and Fig. S3), while polymorph β displays an extremely large aspect ratio with millimetric length and sub-micrometric width and thickness (Fig. 1D-F and Fig. S4). AFM images confirm that the fibrous crystals of polymorph β possess a height of about 70 nm and a width of 500 nm, while the crystals of polymorph α present a height of 400 nm and a width of 600 nm (Fig. S5 and S6). Furthermore, both nanostructures show a strong birefringence, as observed by polarizing optical microphotographs, indicatives of a high degree of anisotropy (Fig 1B, E) and an intense red emission as evidenced by fluorescence images (Fig. 1C, F).

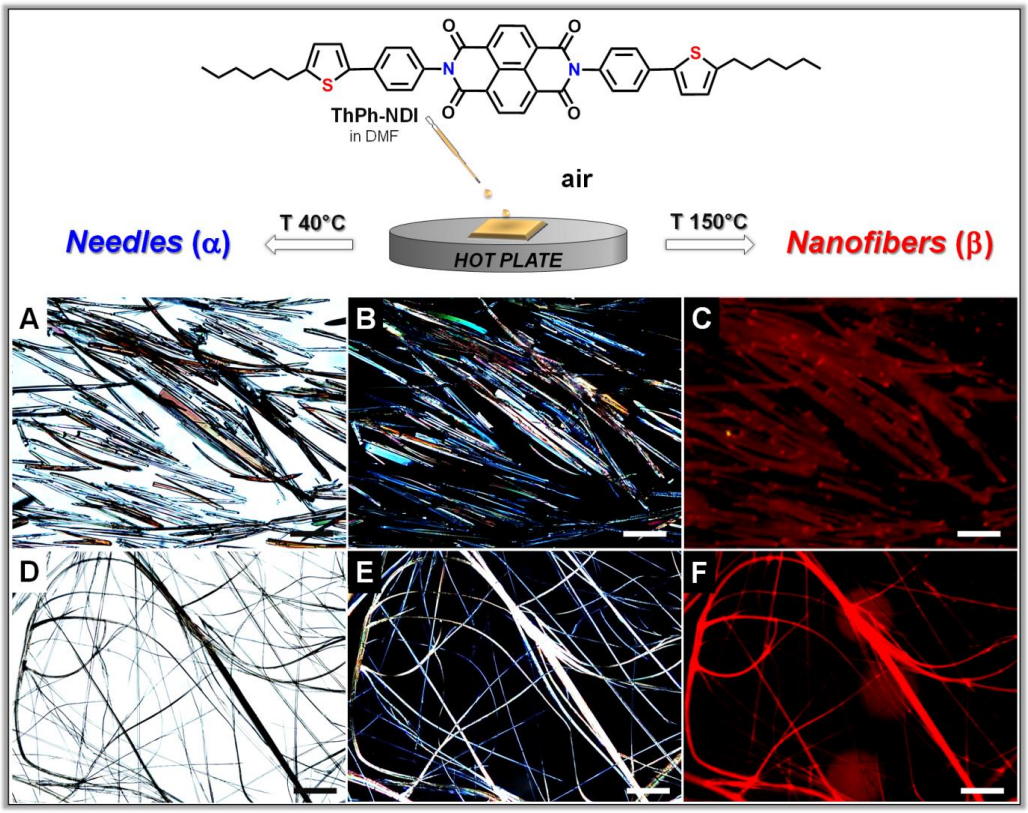

Figure 1. Schematic representation of polymorphs preparation. Needles shaped crystals (A-C) or crystalline nanofibers (D-F) are formed by deposition of a hot DMF solution of **ThPh-NDI** onto a substrate held at a temperature of 40 °C (needles) or 150 °C (nanofibers). Optical microscope images of the two polymorphs under bright field (A, D), cross polarizers (B, E) light illumination and epifluorescence (C, F). Scale bar 10 μm.

DSC analysis performed on both polymorphs suggest that they are monotropically related to one another, given that both polymorphs do not show phase transitions along the entire temperature range up to their melting temperature (Fig. S2). Furthermore, X-ray diffraction analysis indicate that even after 4 years no interconversion between the two forms is observed, thus highlighting that the β polymorph is kinetically trapped and for this reason an appealing system for manufacturing devices with a high operational stability.

Structural characterization. X-ray analysis was performed to elucidate the nature of the exceedingly different morphologies obtained by simply changing the temperature of crystallization. X-ray diffraction (XRD) analysis of thin films of the two nanostructures confirm their high crystallinity and point out the difference between the two phases, as shown by the different diffraction patterns (Fig. 2Aa,c). Both forms were submitted to single crystal investigations succeeding only in the determination of the structure of the α form, since none of the fibers of the β form gave convergent results. We found that the crystal of polymorph α is described by a monoclinic cell $P2_1/c$ with parameters: a = 17.017(2) Å, b = 5.2780(10) Å, c = 21.489(3) Å and β = 103.01(1)° with only half molecule in the asymmetric unit centered on the inversion center (full description of the structure in SI, Table S1, Fig. S7 and S8). As a consequence, the molecular conformation is centrosymmetric with phenyl and thiophene rings lying on the same plane but rotated by 81° respect to the NDI unit, and the alkyl chains in a planar extended conformation. As shown in Figure 2Ba-b, NDI cores present a π-stack interaction with distances of 3.47 Å, although the centroid are 3.95 Å slipped apart, with a slip angle of 41.8° characteristic of a *J*-type arrangement commonly observed in many examples of self-assembled structures based on NDI derivatives.[32-37] The molecular arrangement is characterized by columnar stacks in the direction of the *b* axis (Fig. S9). NDI cores of adjacent

columns are equally oriented respect to the *a,c* plane moving along the *a*-axis direction, but they are inclined in opposite directions moving along the *c* axis (Fig. S9 and S10). Moreover, the rows of columns are interdigitated with the alkyl side chains residing between the NDI cores (Fig. 2Bc). The crystallographic data of polymorph α were used to calculate the powder diffraction profile that better reproduces the experimental one, in order to find the molecular directions respect to the substrate. In Figure 2Ab is reported the pattern calculated in the hypothesis that the (*1 0 0)* and (*-1 0 2)* planes are preferentially oriented parallel to the surface, whose sharp reflections are equal to those of the XRD pattern in thin film (Fig. 2Aa). The corresponding molecular arrangement is shown in Figure 2Bc in which the molecules do not lie flat on the substrate but are inclined from 15° (*-1 0 2* plane) up to 50° (*1 0 0* plane) respect to it. On the other hand, the XRD pattern of the polymorph β shows a profile completely different from that obtained for the α-form with very sharp reflections at angular positions not compatible with the crystal structure of the polymorph α (Fig. 2Ac and inset). In particular, the presence of a reflection at 2θ = 2.42° with a periodicity of 3.6 nm suggests that in polymorph β the molecules are almost parallel to one of the main axis of the unit cell, being the molecular length of about 3.8 nm. This analysis and photophysical properties suggest a disposition of the molecules in a more tightly-packed and overlapped arrangement with a bigger slip angle and a scarce molecular interdigitation (Fig. 2Cc). This may result in the formation of an *H*-type aggregate, characterized by a higher angle between the molecular centroids (*i.e.*, > 54.7°).[38-40] A possible molecular arrangement is graphically sketched in Figure 2Cb.

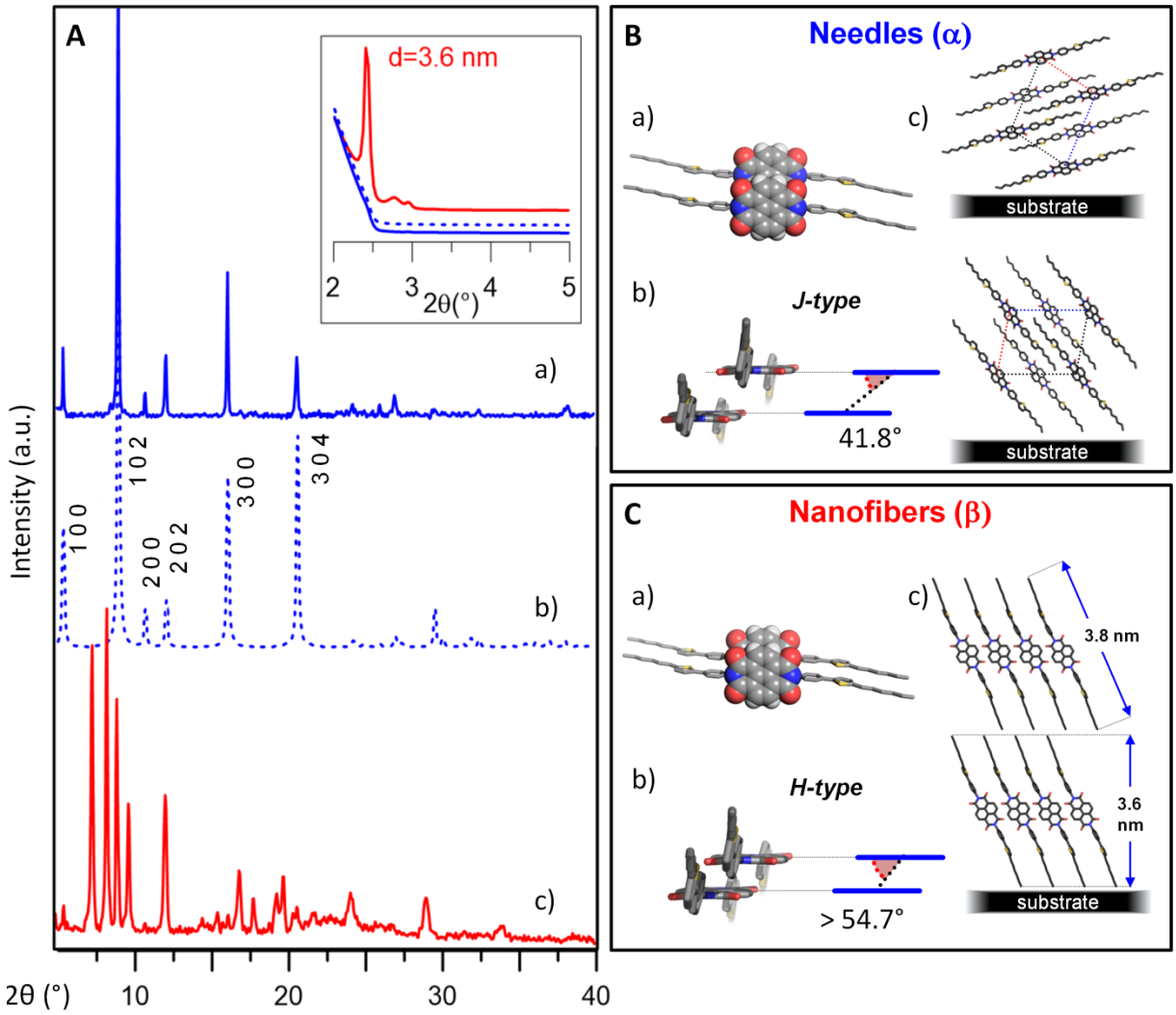

Figure 2. A) XRD patterns: of needles shaped crystals obtained by drop casting at 40°C (a) and calculated from the structure of the single crystal with preferential orientation (*1 0 0)* and (*-1 0 2)* parallel to the surface, Miller indexes of the main reflections are reported (b); of nanofibers obtained by drop casting at 150°C (c). An expanded view of the small angle region is shown in the inset. B) Distances (a) and angles (b) between adjacent molecules in the α form; c) molecular assemblies on a substrate with (*-1 0 2)* or to (*1 0 0)* parallel to the substrate; C) Sketch of the molecular distances (a) and angles (b) between close molecules in the β form; (c) sketch showing possible molecular assemblies on a substrate.

In order to get more quantitative indications about the molecular arrangement of polymorph β, DFT calculations have been carried out to estimate the most energetically-favored slip angle between the individual molecules forming the suggested tightly-packed stacked columns of

polymorph β. The columnar packing was fully optimized at the M06 level of theory in vacuum, as a 1D periodic system, using periodic boundary conditions (PBC) with a single translation vector. The predicted slip angle between the single molecules within the column is 60.6°, characteristic of a H-type arrangement (Fig. 3). Interestingly, the **ThPh-NDI** units do not form a perfectly orthogonal column of molecules, but a tilt angle of 79.8° is observed along the principal axis of the NDI moiety (Fig. S11). In order to consider possible spurious effects due to the basis set superimposition error,[41] counterpoise correction have been considered on model systems based on the corresponding **ThPh-NDI** dimers and trimers (Table S2).[42-43] In any case, no substantial effects were detected and a slip angle of 61° ± 1° can be safely assumed for the columnar packing of polymorph β, strongly validating the hypothesis of a *H*-type aggregate.

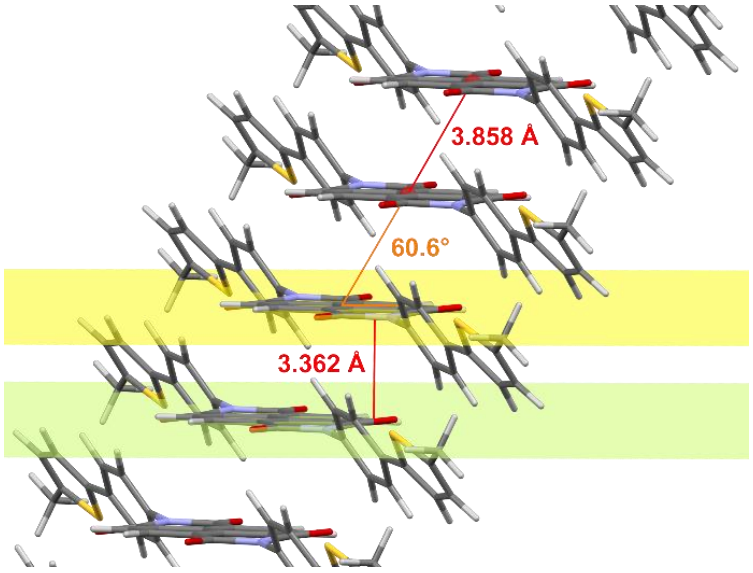

Figure 3. Packing geometry of polymorph β optimized by DFT calculations (assuming a 1D columnar system, using periodic boundary conditions). The relevant structural parameters (*i.e.*, molecular distances and angles) are reported.

Photophysical characterization. ThPh-NDI was characterized in diluted solution, as a dispersion in PMMA and as a solid thin film of both polymorphic nanostructures. The room-temperature absorption spectrum of **ThPh-NDI** as a diluted solution in air-equilibrated DMF (Fig. 4B), presents the typical absorption features of most *N,N*-disubstituted naphtalenediimide dyes, with a vibronically resolved band in the region between 300–400 nm.[44-45] As we argue in detail in the SI (pag. S–20-21), this band corresponds to a π–π* transition centered on the NDI core and attributed to $S_0 \rightarrow S_3$ excitation according to theoretical calculations (Table S3, Fig. S12). Moreover, **ThPh-NDI** displays an extremely weak emission with a photoluminescence quantum yield (PLQY) around $5 \cdot 10^{-5}$ that can be ascribed to emission from the S_3 excited state (Fig. S14).

In thin solid films grown on a quartz substrate, where both polymorphic nanostructures can be prepared and analyzed independently, the α and β forms display absorption spectra which are broadened and slightly red shifted respect to the solution with a series of weak bands extending to over 400 nm (Fig. 4A). Furthermore, the absorption spectra of the two different nanostructures are rather similar, suggesting a comparable HOMO-LUMO energy gap. However, the different electronic interaction in the two crystalline arrangements induces a change in the vibronic progression of the π–π* transition centered on the NDI core determining a difference in the relative intensity of the peaks. According to Spano *et al*.,[46-47] these modifications are diagnostic of the exciton bandwidth and provide an effective way to distinguish J- from H-type aggregates. In particular, the ratio of the oscillator strength of the first two vibronic peaks in the absorption spectrum ($I^{0\text{-}0}_{Abs}/I^{0\text{-}1}_{Abs}$) increases for J-type and decreases for H-type aggregates with exciton bandwidth. Extending this concept to the present case, it is evident that the $I^{0\text{-}0}_{Abs}/I^{0\text{-}1}_{Abs}$ ratio is higher for the needles (α) in agreement with the J-type π stacking motif among the NDI units as

evidenced by the single crystal structure determination, whereas it decreases drastically for the nanofibers (β), where the 0-1 transition band is dominant, pointing to an H-type arrangement as previously suggested by XRD powder diffraction measurements and theoretical calculations.

Most interestingly, the self-assembly profoundly affects the photoluminescence properties of this material inducing an intense solid-state luminescent enhancement (SSE). Indeed, while **ThPh-NDI** is virtually not emissive in diluted solution, thin films of both **ThPh-NDI** polymorphs display an intense double luminescence with two distinct bands: a high energy one, common to both forms and centered at 450 nm, and a second band observed at lower energy with an emission maximum at 650 nm and 750 nm, for the nanofibers (β) and needles (α) respectively.

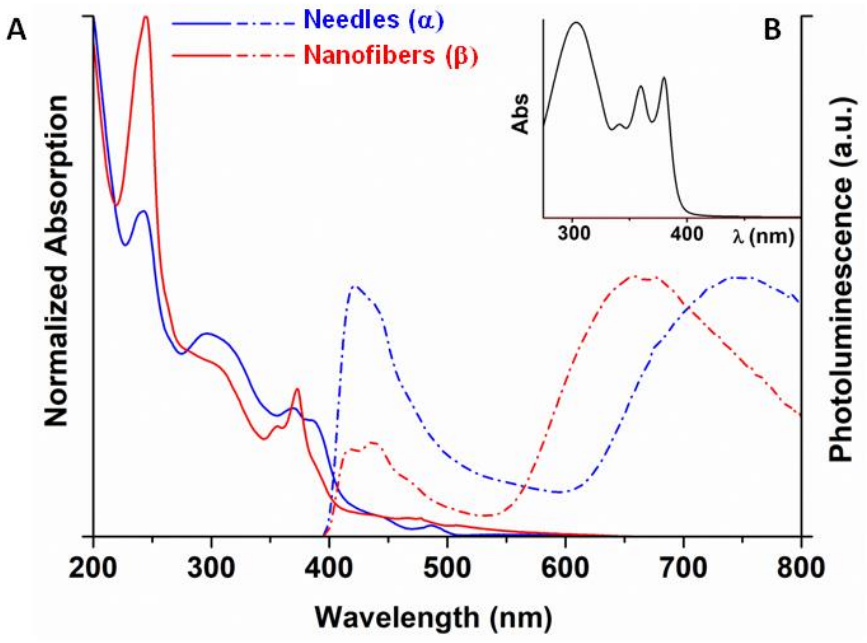

Figure 4. A) Absorption (full line) and emission (dotted line) spectra of thin films of polymorph α (blue) and β (red). λ_{exc} = 380 nm. B) Absorption spectra of **ThPh-NDI** in DMF solution (black).

To better understand the origin of this double luminescence and SSE effect, we recorded the emission spectra of **ThPh-NDI** as a dispersion in PMMA at increasing concentrations. We observed that at low concentration (1% w/w) the emission spectrum is dominated by a single structured band with a maximum at 450 nm, while at higher concentration (>3% w/w) a second emission band at lower energy appears, with an intensity which is proportional to the **ThPh-NDI** concentration in the film (Figure S15). The structured emission at 450 nm is attributed to the π-π* state centered on the NDI core (as observed in diluted solutions of **ThPh-NDI**) while the broad and unstructured emission at lower energy appears to originate from an intermolecular interaction between neighboring **ThPh-NDI** molecules. Indeed, the low energy emission band is very sensitive to the different packing between the two nanostructures (*i.e.*, a red shift of more than 0.25 eV is observed passing from the β to the α form). The great sensitivity of the emission to the molecular packing is tentatively attributed to the presence of charge-transfer states, similar to those discussed in detail in the SI for the diluted solution. The intermolecular interaction that gives origin to the charge transfer state seems to be present already in the ground state as a result of the closeness of packing of **ThPh-NDI** molecules, making the low energy luminescence not imputable to an excimer-like emission as often reported in literature.[48-51] Indeed, excitation-emission maps (Fig. S16), recorded in thin films of both nanostructures, show that the relative intensity of the two emission bands change by changing the excitation wavelength thus ruling out an excimer type luminescence. As a consequence, the ratio between the area of the two emission bands is a rough quantitative indication of the degree of intermolecular coupling present in the ground state of the two different polymorphic forms. The larger area of the 650 nm band compared to that at 450 nm in the emission spectra of polymorph β support the hypothesis of an H-type aggregation geometry that favors a higher degree of π–π stacking between the individual

molecules. In agreement, a blue shift of almost 100 nm is observed in the maximum of the luminescence band at longer wavelength in the β polymorph. Fluorescent H-aggregates of rylene dyes (NDIs, PDIs and others) are uncommon,[52] and to the best of our knowledge this is the first report of two nanostructured polymorphs of an NDI derivative with such markedly different photophysical properties. It is also important to note that polymorphic forms exhibiting solid-state fluorescence in the red and near IR with such a large difference in the emission wavelength are quite rare and intensely sought after for biomedical applications.

Electrochemical characterization. The electrochemical redox properties of **ThPh-NDI** in solution and as polymorphic nanostructures were investigated by cyclic voltammetry (Table S4). In solution, **ThPh-NDI** (Fig. S17) shows two quasi-reversible one-electron reduction waves, with onset at -0.54 V and -0.97 V *vs.* SCE, corresponding to the sequential reduction of the NDI moiety to the radical anion and dianion. Moreover, an irreversible oxidation wave, with the onset potential at 1.5 V, is detected. This relatively low oxidation potential is uncommon for NDIs without electron-donating substituents at the core.[53] However, it can be rationalized considering that the phenyl-thiophene moieties at the imide termini provide relatively high HOMO and HOMO–1 to the molecule. In agreement, DFT calculations estimate the first oxidation process to take place at 1.62 V *vs.* SCE and clearly indicate that it is centered on the phenyl-thiophene substituents, as shown by the spin-density distribution calculated for the corresponding radical cation of **ThPh-NDI** (Fig. S13). Upon oxidation, the phenyl and thiophene rings become almost coplanar with a shortening of the bond distance from 1.46 to 1.44 Å, while their dihedral angle respect to the NDI plane decreases from 75.4° to 64.9°.

On the other hand, in the solid state, both polymorphic nanostructures exhibit a higher oxidation potential (> 1.5 V), probably due to the lack of solvation effects and to the presence of

strong π-π interactions limiting structural rearrangements of the molecule that occur upon oxidation (see above). Additionally, a quasi-reversible bi-electronic reduction wave at onset potentials of -0.95 V for polymorph α and -0.75 V for polymorph β indicate a greater stabilization of the LUMO energy level (*i.e.* a greater electron affinity) for polymorph β (Fig. 5A).

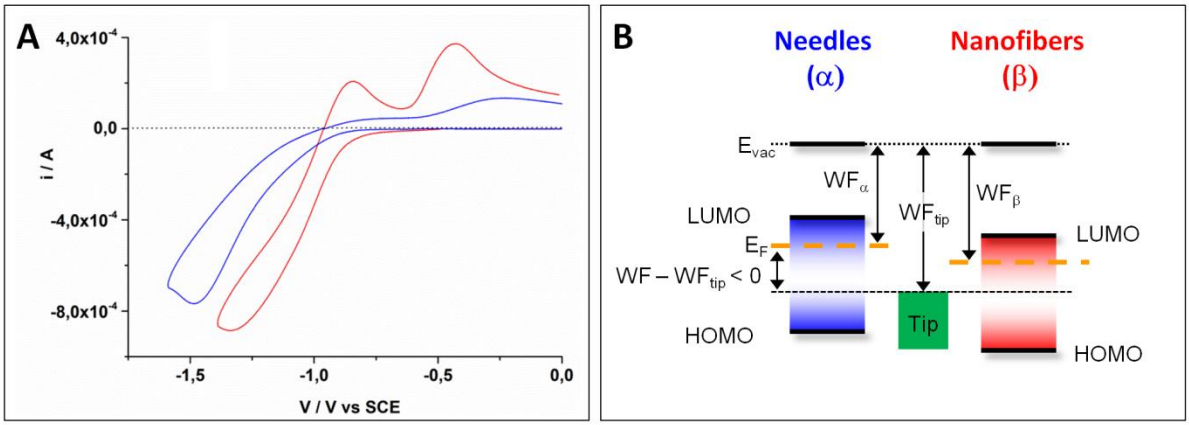

Figure 5. A) voltammograms of polymorph α (blue line) and polymorph β (red line) growth on an ITO substrate. B) Energetics of the two polymorphs respect to the tip work function (WF).

Kelvin Probe Force Microscopy The electronic properties of the two polymorphs were also investigated by Kelvin Probe Force Microscopy (KPFM). The use of this technique allows to quantify at the nanometer scale the surface work function (WF) of the material, i.e. the minimal energy required to extract a bounded electron, that correspond to the difference between the Fermi level of a metal, E_F, and the vacuum level, E_V.[54] In general, the measured values are referred to the tip, thus we define the measured potential (CPD) as the difference of the work function between the sample and the tip ($CPD = WF_{sample} - WF_{tip}$). Moreover, by illuminating the sample with white light, we monitored in-situ the surface photovoltage (SPV) investigating the eventual presence of dipoles at the material surface. We found that the differences in the

molecular packing strongly affect the energetic of the two polymorphs, indeed, the corresponding WF values show a difference amounting to $WF_\beta - WF_\alpha = 220 \pm 20$ meV, with polymorph β exhibiting a lower CPD and consequently a higher work function than polymorph α. The energetic scheme is reported in Figure 5B. As previously described, UV-vis absorption spectra do not show remarkable differences indicating that the HOMO-LUMO energy gap of the two polymorphs is comparable. Thus, changes in the WF values correspond to a "rigid shift" of the electronic levels, which can be ascribed to a different charge distribution at the surface of the two supramolecular architectures in agreement with CV measurements. This assumption is also confirmed by measuring different SPV for the two polymorphs, i.e. the difference between the CPD measured illuminating the sample and in dark: $CPD_{light} - CPD_{dark}$, amounting to 230 ± 10 meV and 170 ± 10 meV, respectively for α (needles) and β (nanofibers) polymorphs. Moreover, in both cases the positive SPV values as well as the lower WFs, compared to the value of the tip used as reference, confirm the *n*-type character of both molecular assemblies. It is noteworthy to underline that the measured difference in the WFs is similar to the energy shift between the emissions maxima of the two polymorphs. This experimental evidence suggests a direct correlation between the work function and the energy of the surface electrons. Further investigations are planned to clarify this issue.

Field Effect Transistor. Owing to the remarkable difference in morphology and crystal packing of the two polymorphs we investigated their charge transport characteristic using them as the active layer in organic field-effect transistors (OFETs). OFETs were built in a bottom-gate, bottom contact architecture: crystalline needles and fibers were simply grown randomly without the need to exclude ambient atmosphere on interdigitated gold source and drain microelectrodes prefabricated on an octadecyltrichlorosilane (OTS) self-assembled monolayer

(SAM) Si/SiO_2 substrate. As demonstrated by transfer in the saturation regime and output characteristics (Fig. 6), both nanostructures unveil air stable n-channel field-effect characteristics with saturated electron mobility, μ_{sat}, up to 2.7×10^{-4} cm^2 V^{-1} s^{-1}, threshold voltage 42 V and on/off ratio 10^3, in the case of the polymorph α and μ_{sat}, up to 5.3×10^{-3} cm^2 V^{-1} s^{-1}, threshold voltage 51 V and on/off 10^3, for the polymorph β. The mobility of the kinetically trapped polymorph (nanofibers) is one order of magnitude higher than that of the thermodynamic one (needles) this can be related to their different assembly and spatial arrangement at the molecular level.[55] It has been recently reported that H-aggregates of NDIs and perylene diimides display n-type mobilities which are between one and two orders of magnitude higher than those of the corresponding J-aggregates.[56-58] According to this, the greater mobility measured for the nanofibers corroborates our hypothesis of their H-type arrangement. It is worth noting that the mobility values in these systems could be largely enhanced by controlling alignment and density, [59-61] however, at this stage, our main aim was to investigate the differences intrinsic to the two nanostructures.

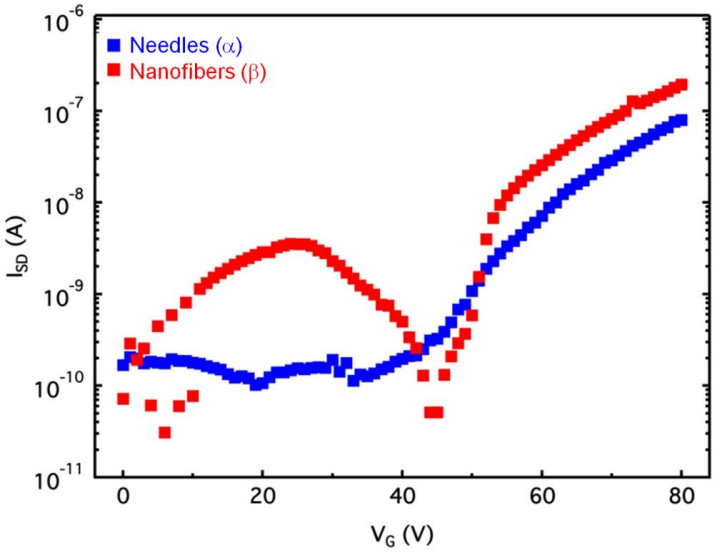

Figure 6. Transfer at drain voltage V_{SD} = 80 V of an OFETs functionalized with OTS and based on polymorph α (blue line) and polymorph β (red line).

CONCLUSIONS

In the present work we show that by simply changing the deposition temperature it is possible to control the aggregation pathway of an NDI-Thiophene derivative. Indeed, two markedly different 1D nanostructures are obtained: needles shaped crystals, grown under thermodynamic control (polymorph α) at low temperature, and nanofibers, formed at high temperature under kinetic control (polymorph β). The two nanostructures, which can be reproducibly grown in pure form on different substrates, present a *J- type* molecular packing in the case of polymorph α, as confirmed by X-ray single analysis, or a *H-type* arrangement for polymorph β as suggested on the basis of theoretical calculations and powder diffraction investigations. Moreover, both polymorphs present an intense solid-state emission enhancement with a double emission originating from a charge transfer state that is strongly influenced by the molecular packing. Intriguingly, we found that the β form exhibits i) an exceptionally high persistence, ii) a lower HOMO and LUMO energy level and iii) superior performances in OFET devices. We believe that this study highlights the importance of accurately screening for novel kinetically trapped polymorphic nanostructures, also for well-known materials. Indeed, novel polymorphic forms, even if metastable, can be persistent in their local energy minimum for a period that greatly exceed the lifetime of a device and show better performances for a given application. Research in this field is expected to open the door to the preparation of a wide variety of new architectures, even from already investigated moieties, with unpredictable emergent properties and applications.

EXPERIMENTAL SECTION

See SI for full synthetic details and characterizations. TGA, DSC, photophysical data, AFM, optical microscope images, additional electrochemical and computational data.

ASSOCIATED CONTENT

The Supporting Information is available free of charge on the ACS Publications website

AUTHOR INFORMATION

Corresponding Author

* E-mail: francesca.dimaria@nanotec.cnr.it (FDM)

* E-mail: massimo.baroncini@unibo.it (MB)

Author Contributions

‖M. Zangoli, M. Gazzano and F. Monti contributed equally to this work.

Notes

The authors declare no competing financial interest.

ACKNOWLEDGMENT

This work was supported by the Progetto FISR – C.N.R. 'TECNOMED - Tecnopolo di Nanotecnologia e Fotonica per la Medicina di Precisione' – CUP B83B17000010001. F.D.M, acknowledge financial support from the UE project INFUSION (Engineering optoelectronic INterfaces: a global action intersecting FUndamental conceptS and technology implementatION of self-organized organic materials, Proposal number: 734834).

ABBREVIATIONS

PDI, Perylene diimmide; DMF, N,N-dimetilformammide; FET, field effect transistor; HOMO-LUMO, highest occupied molecular orbital and lowest unoccupied molecular orbital, respectively.

REFERENCES

(1) Lehn, J. M., Supramolecular Chemistry - Concepts and Perspectives, *Wiley- VCH*, Weinheim, **1995**.

(2) Amabilino, D. B.; Smith, D. K.; Steed, J.W. Supramolecular Materials. *Chem. Soc. Rev*. **2017**, *46*, 2404–2420.

(3) Whitesides, G. M.; Grzybowski, B. Self-Assembly at All Scales. *Science* **2002**, *295*, 2418–2421.

(4) Kim, F. S.; Ren, G.; Jenekhe, S. A. One-Dimensional Nanostructures of π-Conjugated Molecular Systems: Assembly, Properties, and Applications from Photovoltaics, Sensors, and Nanophotonics to Nanoelectronics. *Chem. Mater*. **2011**, *23*, 682–732.

(5) Di Maria, F.; Zangoli, M.; Gazzano, M.; Fabiano, E.; Gentili, D. Zanelli, A.; Fermi, A.; Bergamini, G.; Bonifazi, D.; Perinot, A.; Caironi, M.; Mazzaro, R.; Morandi, V.; Gigli, G.; Liscio, A.; Barbarella, G. Controlling the Functional Properties of Oligothiophene 1D Crystalline Fibers *via* Tailoring of the Self-Assembling Molecular Components. *Adv. Funct. Mater*. **2018**, *28*, 1801946.

(6) Stupp, S. I.; Palmer L. C. Supramolecular Chemistry and Self-Assembly in Organic Materials Design. *Chem. Mater*. **2014**, 26, 507–518.

(7) Ariga, K.; Kunitake, T. Supramolecular Chemistry - Fundamentals and Applications, *Springer*, Heidelberg, **2006**.

(8) Samorì, P.; Biscarini, F. Nanomaterials Properties Tuned by their Environment: Integrating Supramolecular Concepts into Sensing Devices. *Chem. Soc. Rev*. **2018**, *47*, 4675–4676.

(9) Ozin, G. A.; Hou, K.; Lotsch, B. V.; Cademartiri, L.; Puzzo, D. P.; Scotognella, F.; Ghadimi, A.; Thomson, J. Nanofabrication by Self-assembly. *Mater. Today* **2009**, *12*, 12–23.

(10) Avinash, M. B.; Govindaraju, T. Architectonics: Design of Molecular Architecture for Functional Applications. *Acc. Chem. Res.* **2018**, *51*, 414–426.

(11) Aliprandi, A.; Mauro, M.; De Cola L. Controlling and Imaging Biomimetic Self-assembly. *Nat. Chem.* **2016**, *8*, 10–15.

(12) Desiraju, G. Supramolecular Synthons in Crystal Engineering - a New Organic-synthesis. Angew. Chem., Int. Ed. Engl. 1995, 34, 2311− 2327.

(13) Chi, X.; Guerin, A. J.; Haycock, R. A.; Hunter, C. A.; Sarson, L. D. The Thermodynamics of Self-assembly. *J. Chem. Soc., Chem. Commun.* **1995**, 24, 2563−2565.

(14) Lehn, J. M. Toward Self-Organization and Complex Matter. *Science* **2002**, *295*, 2400–2403.

(15) Mattia, E.; Otto, S. Supramolecular Systems Chemistry. *Nat. Nanotechnol.* **2015**, *10*, 111–119.

(16) Korevaar, P. A.; de Greef, T. F. A.; Meijer, E. W. Pathway Complexity in π-Conjugated Materials. *Chem. Mater*. **2014**, *26*, 576–586.
(17) Yan, Y.; Huang, J.; Tang, B. Z. Kinetic Trapping – a Strategy for Directing the Self-Assembly of Unique Functional Nanostructures. *Chem. Commun.* **2016**, *52*, 11870–11884.
(18) Grzybowski, B. A.; Fitzner, K.; Paczesny, J.; Granick, S. From Dynamic Self-assembly to Networked Chemical Systems. *Chem. Soc. Rev.* **2017**, *46*, 5647–5678.
(19) Brown, R. D.; Corcelli, S. A.; Kandel, S. A. Structural Polymorphism as the Result of Kinetically Controlled Self-Assembly. *Acc. Chem. Res.* **2018**, *51*, 465–474.
(20) Belenguer, A. M.; Cruz-Cabeza, A. J.; Lampronti, G. I; Sanders, J. K. M. On the Prevalence of Smooth Polymorphs at the Nanoscale: Implications for Pharmaceuticals. *Cryst. Eng. Comm.* **2019**, *21*, 2203–2211.
(21) Belenguer, A. M.; Lampronti, G. I; Cruz-Cabeza, A. J.; Hunter, C. A.; Sanders, J. K. M. Solvation and Surface Effects on Polymorph Stabilities at the Nanoscale. *Chem. Sci.* **2016**, *7*, 6617–6627.
(22) Li, Q.; Niu, W.; Liu, X.; Chen, Y.; Wu, X.; Wen, X.; Wang, Z.; Zhang, H.; Quan, Z. Pressure-Induced Phase Engineering of Gold Nanostructures. *J. Am. Chem. Soc.* **2018**, *140*, 15783–15790.
(23) Chung, H.; Diao *Y.* Polymorphism as an Emerging Design Strategy for High Performance Organic Electronics. *J. Mater. Chem. C* **2016**, 4, 3915–3933.
(24) Di Maria, F.; Fabiano, E.; Gentili, D.; Biasiucci, M.; Salzillo, T.; Bergamini, G.; Gazzano, M.; Zanelli, A.; Brillante, A.; Cavallini, M.; Della Sala, F.; Gigli, G.; Barbarella, G. Polymorphism in Crystalline Microfibers of Achiral Octithiophene: The Effect on Charge Transport, Supramolecular Chirality and Optical Properties. *Adv. Funct. Mater.* **2014**, *31*, 4943–4951.
(25) Riera-Galindo, S.; Tamayo, A.; Mas-Torrent, M. Role of Polymorphism and Thin-Film Morphology in Organic Semiconductors Processed by Solution Shearing. *ACS Omega* **2018** *3*, 2329–2339.
(26) Al Kobaisi, M.; Bhosale, S. V.; Latham, K.; Raynor, A. M.; Bhosale S. V. Functional Naphthalene Diimides: Synthesis, Properties, and Applications. *Chem. Rev.* **2016**, *116*, 11685−11796.
(27) Weil, T.; Vosch, T.; Hofkens, J.; Peneva, K.; Müllen, K. The Rylene Colorant Family-Tailored Nanoemitters for Photonics Research and Applications. *Angew. Chem. Int. Ed*. **2010**, 49, 9068−9093.
(28) Zhan, X.; Facchetti, A.; Barlow, S.; Marks, T. J.; Ratner, M. A.; Wasielewski, M. R.; Marder, S. R. Rylene and Related Diimides for Organic Electronics. *Adv. Mater.* **2011**, *23*, 268−284.
(29) Gawrys, P.; Djurado, D.; Rimarčík, J.; Kornet, A.; Boudinet, D.; Verilhac, J. M.; Lukeš, V.; Wielgus, I.; Zagorska, M.; Pron, A. Effect of N-Substituents on Redox, Optical, and Electronic Properties of Naphthalene Bisimides Used for Field-Effect Transistors Fabrication. *J. Phys. Chem. B* **2010,** *114*, 1803–1809.

(30) Gawrys, P.; Boudinet, D.; Kornet, A.; Djurado, D.; Pouget, S.; Verilhac, J. M.; Zagorska, M.; Pron, A. Organic Semiconductors for Field-Effect Transistors (Fets): Tuning of Spectroscopic, Electrochemical, Electronic and Structural Properties of Naphthalene Bisimides *via* Substituents Containing Alkylthienyl Moieties. *J. Mater. Chem.* **2010**, *20*, 1913–1920.
(31) Ostwald, W. Studien über die Bildung und Umwandlung fester Körper. *Z. Phys. Chem.* **1897**, *22*, 289–330.
(32) Spano, F. C. The Spectral Signatures of Frenkel Polarons in H- and J-Aggregates. *Acc. Chem. Res.* **2010**, *43*, 429–439.
(33) Mukhopadhyay, P.; Iwashita, Y.; Shirakawa, M.; Kawano, S. I.; Fujita, N.; Shinkai, S. Spontaneous Colorimetric Sensing of the Positional Isomers of Dihydroxynaphthalene in a 1D Organogel Matrix. *Angew. Chem. Int. Ed*., **2006**, *45*, 1592–1595.
(34) Shao, H.; Seifert, J.; Romano, N. C.; Gao, M.; Helmus, J. J.; Jaroniec, C. P.; Modarelli, D. A.; Parquette, J. R. Amphiphilic Self- Assembly of an n- Type Nanotube. *Angew. Chem. Int. Ed*. **2010**, *49*, 7688–7691.
(35) Shao, H.; Parquette, J. R. A π-conjugated Hydrogel Based on an Fmoc-Dipeptide Naphthalene Diimide Semiconductor. *Chem.Commun*. **2010**, *46*, 4285–4287.
(36) Nalluri, S. K. M.; Berdugo, C.; Javid, N.; Frederix, P. W. J. M.; Ulijn, R.V. Biocatalytic Self- Assembly of Supramolecular Charge- Transfer Nanostructures Based on n- Type Semiconductor- Appended Peptides. *Angew. Chem., Int. Ed.* **2014**, *53*, 5882–5887.
(37) Weil, T.; Vosch, T.; Hofkens, J.; Peneva, K.; Müllen, K. The Rylene Colorant Family-Tailored Nanoemitters for Photonics Research and Applications. *Angew. Chem. Int. Ed.* **2010**, *49*, 9068–9093.
(38) Hestand, N. J.; Spano, F. C. Expanded Theory of H- and J-Molecular Aggregates: The Effects of Vibronic Coupling and Intermolecular Charge Transfer. *Chem. Rev.* **2018**, *118*, 7069–7163.
(39) Kasha, M.; Rawls, H. R.; El-Bayoumi, M. A. The Exciton Model in Molecular Spectroscopy. *Pure App. Chem.* **1965**, *11*, 371–392.
(40) Kasha, M. Energy Transfer Mechanisms and the Molecular Exciton Model for Molecular Aggregates. *Radiat. Res.* **1963**, *20*, 55–70.
(41) Liu, B.; McLean, A. D. Accurate Calculation of the Attractive Interaction of two Ground State Helium Atoms. *J. Chem. Phys.* **1973**, *59*, 4557.
(42) Boys, S. F.; Bernardi F. The Calculation of Small Molecular Interactions by the Differences of Separate Total Energies. Some Procedures with Reduced Errors. *Molecular Physics* **1970**, *19*, 553–566.
(43) Simon, S.; Duran, M. How does Basis Set Superposition Error Change the Potential Surfaces for Hydrogen- Bonded Dimers? *J. Chem. Phys.* **1996**, *105*, 11024.
(44) Molla, M. R.; Ghosh S. Hydrogen- Bonding- Mediated J- Aggregation and White- Light Emission from a Remarkably Simple, Single- Component, Naphthalenediimide Chromophore. *Chem. Eur. J.* **2012**, *18*, 1290–1294.

(45) Kalita, A.; Subbarao, N. V. V.; Iyer, P. K. Large-Scale Molecular Packing and Morphology-Dependent High Performance Organic Field-Effect Transistor by Symmetrical Naphthalene Diimide Appended with Methyl Cyclohexane. *J. Phys. Chem. C* **2015**, *119*, 12772–12779.
(46) Hestand, N. J.; Spano, F. C. Expanded Theory of H- and J-Molecular Aggregates: The Effects of Vibronic Coupling and Intermolecular Charge Transfer. *Chem. Rev.* **2018**, *118*, 7069–7163.
(47) Kumar, M.; George, S.J. Spectroscopic Probing of the Dynamic Self- Assembly of an Amphiphilic Naphthalene Diimide Exhibiting Reversible Vapochromism. *Chem. Eur. J.* **2011**, 17, 11102–11106.
(48) Liang, X.; Tan, L.; Liu, Z.; Ma, Y.; Zhang, G.; Wang, L.; Li, S.; Dong, L.; Li, J. Chen W. *Chem. Commun. (Camb.)* **2017**, *53*, 4934–4937.
(49) Barros, T. C.; Brochsztain, S.; Toscano, V. G.; Filhoh, P. B.; Politi, M. J. Photophysical Characterization of a 1,4,5,8-naphthalenediimide Derivative. *J. Photochem. Photobiol. A* **1997**, *111*, 97–104.
(50) Pandeeswar, M.; Govindaraju, T. Bioinspired Nanoarchitectonics of Naphthalene Diimide to Access 2D Sheets of Tunable Size, Shape, and Optoelectronic Properties. *J. Inorg. Organomet. Polym.* **2014**, *25*, 293–300.
(51) Ozser, M. E.; Yucekan, I.; Bodapati, J. B.; Icil, H. New Naphthalene Polyimide with Unusual Molar Absorption Coefficient and Excited State Properties: Synthesis, Photophysics And Electrochemistry. *J. Lumin.* **2013**, *143*, 542–550.
(52) Basak, S.; Nandi, N.; Bhattacharyya, K.; Datta, A.; Banerjee, A. Fluorescence from an H-Aggregated Naphthalenediimide Based Peptide: Photophysical and Computational Investigation of this Rare Phenomenon. *Phys. Chem. Chem. Phys.* **2015**, *17*, 30398–30403.
(53) Sakai, N.; Mareda, J.; Vauthey E.; Matile S. Core-substituted Naphthalenediimides. *Chem. Commun.* **2010**, *46*, 4225–4237.
(54) Liscio, A.; Palermo, V.; Samorí, P. Nanoscale Quantitative Measurement of the Potential of Charged Nanostructures by Electrostatic and Kelvin Probe Force Microscopy: Unraveling Electronic Processes in Complex Materials**.** *Acc. Chem. Res.* **2010**, *43*, 541–550.
(55) Brédas, J. L.; Calbert, J. P.; da Silva Filho D. A.; Cornil J. Organic Semiconductors: a Theoretical Characterization of the Basic Parameters Governing Charge Transport. *Proc. Natl Acad. Sci. USA* **2002**, *99*, 5804–5809.
(56) He, T.; Stolte, M.; Burschka, C.; Hansen, N. H.; Musiol T.; Kälblein, D.; Pflaum, J.; Tao, X.; Brill, J.; Würthner, F. Single-Crystal Field-Effect Transistors of new Cl_2-NDI Polymorph Processed by Sublimation in Air. *Nat. Commun.* **2015**, *6*, 5954.
(57) Kim, S. O.; An, T. K.; Chen, J.; Kang, I.; Kang, S. H.; Chung, D. S.; Park, C. E.; Kim, Y. H.; Kwon, S. K. H- Aggregation Strategy in the Design of Molecular Semiconductors for Highly Reliable Organic Thin Film Transistors. *Adv. Funct. Mater.* **2011**, *21*, 1616–1623.
(58) Chen, Y.; Feng, Y.; Gao, J.; Bouvet M. Self-Assembled Aggregates of Amphiphilic Perylene Diimide–Based Semiconductor Molecules: Effect of Morphology on Conductivity. *J. Colloid Interface Sci*. **2012**, *368*, 387–394.

(59) Oh, J. H.; Lee, H. W.; Mannsfeld, S.; Stoltenberg, R. M.; Jung, E.; Jin, Y. W.; Kim, J. M.; Yoo, J. B.; Bao, Z. Solution-processed, high-performance n-channel organic microwire transistors. *Proc. Natl. Acad. Sci. USA* **2009**, *106*, 6065–6070.
(60) Gentili, D.; Di Maria, F.; Liscio, F.; Ferlauto, L.; Leonardi, F.; Maini, L.; Gazzano, M.; Milita, S.; Barbarella, G.; Cavallini, M. Targeting Ordered Oligothiophene Fibers with Enhanced Functional Properties by Interplay of Self-assembly and Wet Lithography. *J. Mater. Chem.* **2012**, *22*, 20852–20856.
(61) Hung, A. M.; Stupp, S. I. Simultaneous self-assembly, orientation, and patterning of peptide-amphiphile nanofibers by soft lithography. *Nano Lett.* **2007**, *7*, 1165–1171.
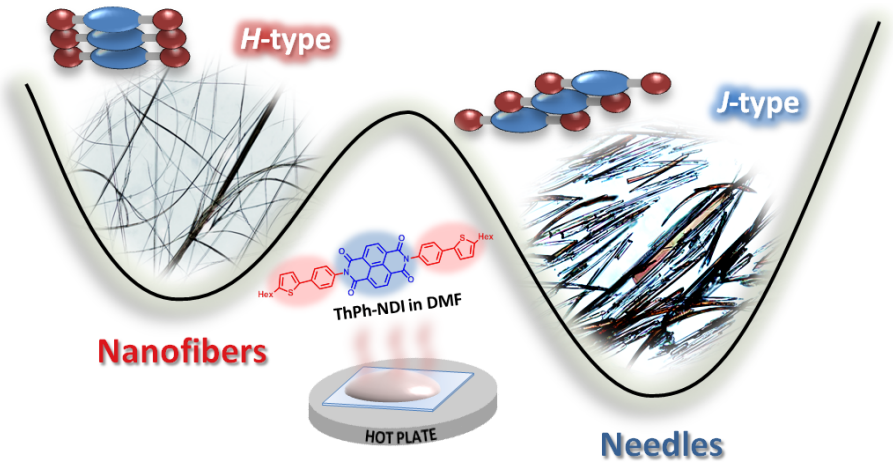
Table of Contents